Heat Transfer Research, 2011, Vol. 42, No. 5

A Theoretical Model for Unsteady Coupled Heat and Mass Transfer Phenomena in Industrial Dryers

H. SHOKOUHMAND,[1] S. BIGHAM,[1*] and S. YAZDANI[2]

[1]School of Mechanical Engineering, College of Engineering, University of Tehran, Tehran, Iran

[2]School of Energy, Kermanshah University of Technology, Kermanshah, Iran

An analytical method is proposed to investigate the combined heat and mass transfer phenomena taking place in industrial dryers. The unsteady heat and mass transfer equations are solved analytically to obtain the distributions of the fluid and solid temperatures and the solid humidity. At the fluid and solid interface, due to the temperature and concentration gradients in the fluid and in the solid, the governing equations are coupled. One of the principal aims of the current research is to propose an analytical method for estimation of the required time for drying of a solid material. For the case of $e = 0.03$ and $\delta = 0.09$, the results show that the solid is dried in approximately 25 min while for the case of $e = 0.5$ and $\delta = 1.5$, the required time of drying is almost 600 min.

* * *

Key words: coupled heat and mass transfer, drying, theoretical solution, eigenvalues, eigenfunctions

1. INTRODUCTION

Drying is a complicated process involving simultaneous heat, mass, and momentum transfer phenomena and effective models are necessary for process design, optimization, energy integration, and control. Drying commonly describes the process of thermal removing volatile substances (moisture) to yield a solid product. Utilization of a

*Address all correspondence to S. Bigham E-mail: sajjadbigham@ut.ac.ir; sajjadbigham@gmail.com

ISSN1064-2285

high amount of energy in the drying industry makes drying one of the most energy-intensive operations with a great industrial significance. Therefore, performing of a drying process in an optimal way is essentially crucial.

Drying is likely the oldest and most common chemical engineering unit operations (Wiliams-Gardner, 1971). Because the weight and the volume of a product become less in its dried form, packaging, handling, and transportation of a dry product are easier and cheaper after drying. Food products are dried for an improved mixing, milling or segregation operation. No doubt that synthetic drug has played a vital role in the enhancement of human living standards. The quality of the herbs depends very much on the contents of active ingredients. It is known that heating or thermal drying, if not carried out properly, can cause a significant loss of the active ingredients. In the preparation of nanoparticles by the liquid-phase method, drying is an indispensable unit operation. The anatomical structure of wood limits how rapidly water can move through and out of wood (Mujumdar, 1995; van Arsdel et al., 1973; Ashworth, 1977). The fact that tens of thousands of products need to be dried in over a hundred of variants of dryers provides major and ample opportunities for innovation.

The transfer of heat and moisture on solid materials was a topic of a considerable research interest in the recent past. There are a number of efforts to develop coupled heat and mass transfer models that are suitable for the design. Many researchers investigated the simultaneous heat and mass transfer, theoretically (Raisul Islam et al., 2006; Papia et al., 2007; Arnaud and Fohr, 1988; Johansson et al., 1997; Kulasiri and Woodhead, 2005), numerically (Talukadr et al., 2008; Le Palec, 1992; Ibrahim and Vinnicombe, 1993), and experimentally (Iskra and Siminson, 2007; Li et al., 2006; Olutimayin and Siminson, 2005). Luikov (1966) showed the importance of the temperature gradient for moisture migration in capillary-porous bodies. He developed a system of coupled PDEs using the thermodynamics of irreversible processes. Olbrich and Wild (1969) provided a solution to the diffusion equation in laminar flow for several falling film geometries. The solution, in the form of a series of eigenfunctions, includes ten eigenvalues and coefficients. Thomas et al. (1980) used the coupled two-dimensional PDEs based on Luikov's theory to develop a fully nonlinear finite element formulation to solve a problem of kiln drying timber having a cross section of 200 mm $\times$ 50 mm. Then they simplified the numerical problem using a linear finite element formulation for the same cross section of timber and concluded that the use of a fully nonlinear formulation was not justified because there was no difference in results from both formulations. Grossman (1983) described a theoretical analysis of the combined heat and mass transfer process taking place in the absorption of a gas or vapor into a laminar liquid film. Killion and Garimella (2001) provided a comprehensive review of the significant efforts that researchers have made to model the coupled heat and mass transfer phenomena mathematically.

The purpose of the present study is to develop an analytical model of the combined heat and mass transfer process taking place in industrial dryers. Equations are coupled at the interfacial boundary condition between the solid and the fluid. By

solving the mentioned equations, the solid humidity distribution and the fluid/solid temperature variations can be found.

2. PROBLEM DESCRIPTION

The physical configuration of the problem under investigation is presented schematically in Fig. 1. This figure shows that a solid slab is horizontally located in a long space in the x direction. The solid is assumed to be wet and cold. It is also supposed that space is occupied by a stationary hot air. Because the space is long in the x direction, the gradient of variations can be neglected in this direction. So, the problem is studied only in the y direction.

At $t = 0$, the air temperature, the solid temperature, and the solid humidity are shown by T_{oa}, T_{os}, and ω_{oa}, respectively. Because the initial air temperature (T_{oa}) is greater than the initial solid temperature (T_{os}), heat transfer occurs from the fluid to the solid body. As time increases, due to heat transfer from the fluid to the solid, the solid temperature increases. During this process, both the solid humidity and the fluid temperature decrease.

3. GOVERNING EQUATIONS

The model consists of a set of equations that describe the heat and mass transfer phenomena within fluid and solid materials. The equations of the model are solved theoretically to calculate the fluid/solid temperature distribution and the solid mass distributions. The list of the assumptions that are used in developing the mathematical model is as follows:

(i) The thermophysical properties of the fluid and the solid are assumed to be constant.
(ii) Heat and mass transfer are considered to be unsteady and one-dimensional in the y direction as mentioned before.
(iii) There are no natural convection effects in the fluid due to temperature or concentration gradients.
(iv) Diffusion thermal effects are negligible.

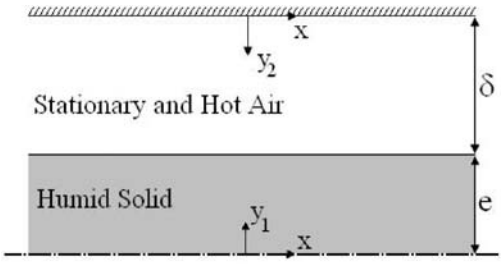

Fig. 1. Schematic of the physical domain.

(v) The concentration is assumed to be very high so that the interfacial temperature, T_{int}, and the solid moisture at the interface, ω_{int}, can be related through the interfacial saturated pressure, P_{sat}, according to the following equation at all times:

$$\omega_{int} = 0.622 \frac{P_{sat}}{P - P_{sat}} , \tag{1}$$

where P is the total vapor pressure and P_{sat} is calculated from the Bertrand formula (Bruhat, 1968):

$$P_{sat} = 10^{(17.433 - 2795/T_{int} - 3.8681 \log_{10}(T_{int}))} . \tag{2}$$

For analytical solution, the above curve is estimated by a linear relation that can be written as:

$$\omega_{int} - \omega_e = \frac{\omega_{os} - \omega_e}{T_e - T_{os}} (T_{int} - T_{os}) , \tag{3}$$

where ω_e is the equilibrium humidity of the solid at the temperature T_{os} and T_e is the equilibrium temperature of the solid at the humidity ω_{os}.

3.1. Energy Equations

As mentioned before, the fluid is stationary and hot. Unsteady and one-dimensional form of the heat equation has, therefore, the following form:

$$\frac{\partial T_a}{\partial t} = \alpha_a \frac{\partial^2 T_a}{\partial y^2} . \tag{4}$$

Unsteady and one-dimensional form of heat conduction through the solid is expressed as:

$$\frac{\partial T_s}{\partial t} = \alpha_s \frac{\partial^2 T_s}{\partial y^2} , \tag{5}$$

where the thermal diffusion term in the x direction has been neglected with respect to that in the y direction.

3.2. Penetration Model

Diffusion into solid materials during drying process is a complex process that may involve molecular diffusion, capillary flow, Knudsen flow, hydrodynamic flow or surface diffusion. If all these phenomena are combined into one, the effective diffusivity can be defined from Fick's second law:

$$\frac{\partial \omega}{\partial t} = D \frac{\partial^2 \omega}{\partial y^2} , \tag{6}$$

where diffusion in the x direction has been neglected with respect to that in the y direction. D, ω, and t are the effective diffusivity, the material moisture content, and time, respectively.

3.3. Boundary Conditions

This set of governing equations has been solved subject to the following boundary conditions:

Line $y_1 = 0$ is a symmetry line and line $y_2 = 0$ is an adiabatic line, therefore:

$$\left(\frac{\partial T_s}{\partial y_1}\right)_{y_1=0} = \left(\frac{\partial T_a}{\partial y_2}\right)_{y_2=0} = \left(\frac{\partial \omega}{\partial y_1}\right)_{y_1=0} = 0. \tag{7}$$

At the interface, the temperatures of the solid and the air are equal so the equilibrium condition exists. It is assumed that the amount of heat that is exerted by air divides into two parts. One of them heats the solid and the other evaporates moisture of the solid. Also, it is assumed that the heat that is required to evaporate the solid humidity is equal to the sensible heat transfer from air to the solid interface, therefore:

$$(T_s)_{y_1=e} = (T_a)_{y_2=\delta}, \tag{8}$$

$$\omega_{int} - \omega_e = \frac{\omega_{os} - \omega_e}{T_e - T_{os}}(T_{int} - T_{os}), \tag{9}$$

$$\left(-k_a \frac{\partial T_a}{\partial y_2}\right)_{y_2=\delta} = -\left(Dh_{gf}\rho_a \frac{\partial \omega}{\partial y_1}\right)_{y_1=e} + \left(k_s \frac{\partial T_s}{\partial y_1}\right)_{y_1=e}. \tag{10}$$

At the initial time, the boundary conditions are:

$$(T_a)_{(y_2,t=0)} = T_{oa}, \tag{11}$$

$$(T_s)_{(y_1,t=0)} = T_{os}, \tag{12}$$

$$(\omega)_{(y_1,t=0)} = \omega_{os}. \tag{13}$$

The governing equations will be non-dimensionalized by implementation of the following non-dimensional terms:

$$\eta_1 = \frac{y_1}{e}, \quad \eta_2 = \frac{y_2}{\delta}, \quad \tau_s = \frac{t\alpha_s}{e^2}, \quad \tau_a = \frac{t\alpha_a}{\delta^2}.$$

Non-dimensional governing equations are found as:

Air non-dimensional energy equation:

$$\frac{\partial \theta_a}{\partial \tau_2} = \frac{\partial^2 \theta_a}{\partial \eta_2^2}. \tag{14}$$

Solid non-dimensional energy equation:

$$\frac{\partial \theta_s}{\partial \tau_1} = \frac{\partial^2 \theta_s}{\partial \eta_1^2}. \tag{15}$$

Solid humidity non-dimensional equation:

$$\frac{\partial \varpi}{\partial \tau_1} = \frac{1}{Le}\frac{\partial^2 \varpi}{\partial \eta_1^2} , \tag{16}$$

where Le is the Lewis number that is defined as Le = α_s/D.

Also, the non-dimensional boundary conditions have the following form:

At $\eta_1 = \eta_2 = 0$

$$\left(\frac{\partial \theta_s}{\partial \eta_1}\right)_{\eta_1=0} = \left(\frac{\partial \theta_a}{\partial \eta_2}\right)_{\eta_2=0} = \left(\frac{\partial \varpi}{\partial \eta_1}\right)_{\eta_1=0} = 0 . \tag{17}$$

At the interface, i.e., $\eta_1 = \eta_2 = 1$

$$(\theta_s)_{\eta_1=1} = (\theta_a)_{\eta_2=1} , \tag{18}$$

$$(\varpi)_{\eta_1=1} + (\theta_s)_{\eta_2=1} = 1 , \tag{19}$$

$$\left(\frac{\partial \theta_a}{\partial \eta_2}\right)_{\eta_2=1} = \lambda_1 \left(\frac{\partial \varpi}{\partial \eta_1}\right)_{\eta_1=1} + \lambda_2 \left(\frac{\partial \theta_s}{\partial \eta_1}\right)_{\eta_1=1} , \tag{20}$$

where η_1 and η_2 are determined as:

$$\lambda_1 = \frac{\delta D \rho_a h_{fg}(\omega_e - \omega_{os}}{e k_a (T_e - T_{os})} , \quad \lambda_2 = -\frac{\delta}{e}\frac{k_s}{k_a} .$$

At the initial time, i.e., $\tau_1 = \tau_2 = 0$, the non-dimensional boundary conditions are

$$(\theta_a)_{(\eta_2,\tau_2=0)} = \lambda_4 , \tag{21}$$

$$(\theta_s)_{(\eta_1,\tau_1=0)} = 0 , \tag{22}$$

$$(\varpi)_{(\eta_1,\tau_1=0)} = 0 , \tag{23}$$

where λ_4 is determined as:

$$\lambda_4 = \frac{(T_{oa} - T_{os})}{(T_e - T_{os})} .$$

The set of equations (14) through (16) will be solved analytically. With respect to the interfacial boundary conditions, the above equations are coupled.

4. ANALYTICAL SOLUTION

By using the method of separating variables for Eq. (14), two ODEs are obtained. Three boundary conditions are required for solving the ODEs. Because one of the

three boundary conditions is coupled at the interface and it is not distinct clearly, the solution of Eq. (14) is coupled with Eqs. (15) and (16).

By using the methods of separating variables and the Fourier series, solutions of Eqs. (14)–(16) with the boundary condition (17), in the form of three infinite series, have the following form:

$$\theta_a = \sum_{n=1}^{\infty} A_n \cos(\alpha_n \eta_2) \exp(-\alpha_n{}^2 \tau_2), \tag{24}$$

$$\theta_s = \sum_{n=1}^{\infty} B_n \cos(\beta_n \eta_1) \exp(-\beta_n{}^2 \tau_1), \tag{25}$$

$$\varpi = \sum_{n=1}^{\infty} C_n \cos(\sqrt{Le}\gamma_n \eta_1) \exp(-\gamma_n{}^2 \tau_1), \tag{26}$$

where α_n, β_n, and γ_n are the eigenvalues.

If Eq. (26) is rewritten in the following form, it will satisfy Eq. (16) and the boundary conditions (17) and (19), again. So, Eq. (26) is changed as:

$$\varpi = 1 - \sum_{n=1}^{\infty} C_n \cos(\sqrt{Le}\gamma_n \eta_1) \exp(-\gamma_n^2 \tau_1) \ . \tag{27}$$

Because Eqs. (24), (25), and (27) must be satisfied by the boundary conditions (18) and (19) at any τ_1 and τ_2, it is obvious that for every n

$$\beta_n = \gamma_n \ , \tag{28}$$

$$\alpha_n = \sqrt{\lambda_3}\ \beta_n \ , \tag{29}$$

where λ_3 is determined as:

$$\lambda_3 = \left(\frac{\alpha_s \delta^2}{\alpha_a e^2} \right) . \tag{30}$$

Also the boundary conditions (18)–(20) exert the following conditions:

$$B_n \cos(\beta_n) = C_n \cos(\sqrt{Le}\beta_n) \, , \tag{31}$$

$$B_n \cos(\beta_n) = A_n \cos(\sqrt{\lambda_3}\beta_n) \, , \tag{32}$$

$$-A_n \sqrt{\lambda_3}\beta_n \sin(\sqrt{\lambda_3}\beta_n) = C_n \lambda_1 \sqrt{Le}\beta_n \sin(\sqrt{Le}\beta_n) - B_n \lambda_2 \beta_n \sin(\beta_n) \, . \tag{33}$$

Equations (31)–(33) are homogeneous for A_n, B_n, and C_n and have a unique solution only if the determinant equals zero, i.e., if

$$-\lambda_1 \sqrt{Le}\beta_n \sin(\sqrt{Le}\beta_n)\cos(\beta_n)\cos(\sqrt{\lambda_3}\beta_n) + \lambda_2 \beta_n \sin(\beta_n)\cos(\sqrt{Le}\beta_n)\cos(\sqrt{\lambda_3}\beta_n)$$

$$-\sqrt{\lambda_3}\beta_n \sin(\sqrt{\lambda_3}\beta_n)\cos(\beta_n)\cos(\sqrt{Le}\beta_n) = 0 \, . \tag{34}$$

By solving Eq. (34), the eigenvalues β_n are determined. Then the eigenvalues α_n and γ_n are found by using Eqs. (28) and (29).

The Sturm-Liouville orthogonality condition and the boundary conditions (21)–(23) are used to find A_n, B_n, and C_n.

Equations (24), (25), and (27) can be rewritten in the form of three infinite series of eigenfunctions F_n, G_n, and H_n as

$$\theta_a = \sum_{n=1}^{\infty} A_n F_n(\eta_2) \exp(-\lambda_3 \beta_n^2 \tau_2), \tag{35}$$

$$\theta_s = \sum_{n=1}^{\infty} B_n G_n(\eta_1) \exp(-\beta_n^2 \tau_1), \tag{36}$$

$$\varpi = 1 - \sum_{n=1}^{\infty} C_n H_n(\eta_1) \exp(-\beta_n^2 \tau_1), \tag{37}$$

where

$$F_n(\eta_2) = \cos(\sqrt{\lambda_3}\beta_n \eta_2),$$

$$G_n(\eta_1) = \cos(\beta_n \eta_1),$$

$$H_n(\eta_1) = \cos(\sqrt{Le}\beta_n \eta_1).$$

By substituting Eqs. (35), (36), and (37) into Eqs. (14), (15), and (16), respectively, three following equations for the eigenfunctions F_n, G_n, and H_n are obtained:

$$\frac{d^2 F_n(\eta_2)}{d\eta_2^2} + \lambda_3 \beta_n^2 F_n(\eta_2) = 0, \tag{38}$$

$$\frac{d^2 G_n(\eta_1)}{d\eta_1^2} + \beta_n^2 G_n(\eta_1) = 0, \tag{39}$$

$$\frac{d^2 H_n(\eta_1)}{d\eta_1^2} + Le\beta_n^2 H_n(\eta_1) = 0. \tag{40}$$

By considering Eq. (38) for the eigenfunction F_n, multiplying it by another eigenfunction F_m and integrating over the range of η_2 we have:

$$\lambda_3 \beta_n^2 \int_0^1 F_n F_m d\eta_2 = -F_n'(1) F_m(1) + \int_0^1 F_n' F_m' d\eta_2. \tag{41}$$

Similarly

$$\lambda_3 \beta_m^2 \int_0^1 F_n F_m d\eta_2 = -F_n(1) F_m'(1) + \int_0^1 F_n' F_m' d\eta_2. \tag{42}$$

By subtracting Eq. (42) from Eq. (41) and using the boundary condition (17), the following equation is obtained:

$$\lambda_3 (\beta_m^2 - \beta_n^2) \int_0^1 F_n F_m d\eta_2 = F_n'(1) F_m(1) - F_n(1) F_m'(1). \tag{43}$$

In the same manner, considering Eqs. (39) and (40) for the eigenfunctions G_n and H_n, two following equations are obtained, respectively:

$$(\beta_m{}^2 - \beta_n{}^2)\int_0^1 G_n G_m d\eta_1 = G_n'(1)G_m(1) - G_n(1)G_m'(1), \tag{44}$$

$$Le(\beta_m{}^2 - \beta_n{}^2)\int_0^1 H_n H_m d\eta_1 = H_n'(1)H_m(1) - H_n(1)H_m'(1). \tag{45}$$

Equations (31), (32), and (33) can be rewritten in the following form:

$$B_n G_n(1) = C_n H_n(1), \tag{46}$$

$$A_n F_n(1) = B_n G_n(1), \tag{47}$$

$$A_n F_n'(1) = \lambda_2 B_n G_n'(1) - \lambda_1 C_n H_n'(1). \tag{48}$$

By combining Eqs. (47) and (48), the following equation is obtained:

$$A_n A_m F_n(1) F_m'(1) = \lambda_2 B_n B_m G_n(1) G_m'(1) - \lambda_1 B_n C_m G_n(1) H_m'(1). \tag{49}$$

Similarly

$$A_n A_m F_n'(1) F_m(1) = \lambda_2 B_n B_m G_n'(1) G_m(1) - \lambda_1 B_m C_n G_m(1) H_n'(1). \tag{50}$$

By subtracting Eq. (50) from Eq. (49) and using Eq. (46), the following equation is obtained:

$$\begin{aligned} A_n A_m (F_n(1)F_m'(1) - F_n'(1)F_m(1)) &= \lambda_2 B_n B_m (G_n(1)G_m'(1) - G_n'(1)G_m(1)) \\ -\lambda_1 (B_n C_m G_n(1) H_m'(1) - B_m C_n H_n'(1) G_m(1)). \end{aligned} \tag{51}$$

By substituting Eqs. (43), (44), and (45) into Eq. (51), the following equation is obtained:

$$\begin{aligned} (\beta_m{}^2 - \beta_n{}^2)(\lambda_3 A_n A_m \int_0^1 F_n F_m d\eta_2 - \lambda_2 B_n B_m \int_0^1 G_n G_m d\eta_1 \\ +\lambda_1 Le C_n C_m \int_0^1 H_n H_m d\eta_1) = 0. \end{aligned} \tag{52}$$

By using the orthogonality condition, Eq. (52) can be written in the following form:

$$\begin{aligned} &\lambda_3 A_n A_m \int_0^1 F_n F_m d\eta_2 - \lambda_2 B_n B_m \int_0^1 G_n G_m d\eta_1 \\ &+\lambda_1 Le C_n C_m \int_0^1 H_n H_m d\eta_1 \begin{cases} = 0 & \text{for } n \neq m \\ \neq 0 & \text{for } n = m \end{cases} \end{aligned} \tag{53}$$

At this point, we return to the boundary conditions (21) through (23) and using Eqs. (35)–(37), the following equations are found:

$$\sum_{n=1}^{\infty} A_n A_m F_n(\eta_2) F_m(\eta_2) = \lambda_4 A_m F_m(\eta_2), \tag{54}$$

$$\sum_{n=1}^{\infty} B_n B_m G_n(\eta_1) G_m(\eta_1) = 0, \tag{55}$$

$$\sum_{n=1}^{\infty} C_n C_m H_n(\eta_1) H_m(\eta_1) = C_m H_m(\eta_1). \tag{56}$$

By integrating Eqs. (54), (55), and (56) over their specific range [i.e., the range of η_2 for Eq. (54) and the range of η_1 for Eqs. (55) and (56)] and combining the obtained equations, the following equation is obtained:

$$\lambda_3 \sum_{n=1}^{\infty} A_n A_m \int_0^1 F_n(\eta_2) F_m(\eta_2) d\eta_2 - \lambda_2 \sum_{n=1}^{\infty} B_n B_m \int_0^1 G_n(\eta_1) G_m(\eta_1) d\eta_1 \tag{57}$$

$$+\lambda_1 Le \sum_{n=1}^{\infty} C_n C_m \int_0^1 H_n(\eta_1) H_m(\eta_1) d\eta_1 = \lambda_3 \lambda_4 A_m \int_0^1 F_m(\eta_2) d\eta_2 + \lambda_1 Le C_m \int_0^1 H_m(\eta_1) d\eta_1 .$$

By combining Eqs. (53) and (57), the following equation is obtained:

$$\lambda_3 A_n^{\,2} \int_0^1 F_n^{\,2}(\eta_2) d\eta_2 - \lambda_2 B_n^{\,2} \int_0^1 G_n^{\,2}(\eta_1) d\eta_1 + \lambda_1 Le C_n^{\,2} \int_0^1 H_n^{\,2}(\eta_1) d\eta_1$$

$$= \lambda_3 \lambda_4 A_n \int_0^1 F_n(\eta_2) d\eta_2 + \lambda_1 Le C_n \int_0^1 H_n(\eta_1) d\eta_1 . \tag{58}$$

Equation (58) provides one relation between A_n, B_n, and C_n; the two other relations between them are available in Eqs. (31) and (32). Solution of Eqs. (31), (32), and (58) for A_n, B_n, and C_n yields the following equations:

$$A_n = \{\lambda_3 \lambda_4 \int_0^1 \cos(\sqrt{Le}\beta_n \eta_2) d\eta_2$$

$$+\lambda_1 Le \left(\frac{\cos(\sqrt{\lambda_3}\beta_n)}{\cos(\sqrt{Le}\beta_n)}\right) \int_0^1 \cos(\sqrt{Le}\beta_n \eta_1) d\eta_1 \} / \{\lambda_3 \int_0^1 \cos^2(\sqrt{\lambda_3}\beta_n \eta_2) d\eta_2$$

$$-\lambda_2 \left(\frac{\cos(\sqrt{\lambda_3}\beta_n)}{\cos(\beta_n)}\right)^2 \int_0^1 \cos^2(\beta_n \eta_1) d\eta_1 + \lambda_1 Le \left(\frac{\cos(\sqrt{\lambda_3}\beta_n)}{\cos(\sqrt{Le}\beta_n)}\right)^2 \int_0^1 \cos^2(\sqrt{Le}\beta_n \eta_1) d\eta_1 \}, \tag{59}$$

$$B_n = A_n \left(\frac{\cos(\sqrt{\lambda_3}\beta_n)}{\cos(\beta_n)}\right), \tag{60}$$

$$C_n = A_n \left(\frac{\cos(\sqrt{\lambda_3}\beta_n)}{\cos(\sqrt{Le}\beta_n)}\right). \tag{61}$$

The analytical solution is now completed. As summary, the temperature distribution of the air and the solid are obtained from Eqs. (24) and (25), respectively. The solid humidity is calculated from Eq. (27). The eigenvalues β_n are achieved by solving Eq. (34). In addition, the coefficients A_n, B_n, and C_n are determined by Eqs. (59), (60), and (61).

5. RESULTS AND DISCUSSION

In order to have a physical point of view of the problem, the analytical solution achieved in the previous sections is applied for typical values of the parameters: k_a = 0.0263 [W·m^{-1}·^{o}C^{-1}], k_s = 0.166 [W·m^{-1} ^{o}C^{-1}], $\alpha_a = 0.2216 \times 10^{-4}$ [m^2·s^{-1}], $\alpha_s = 1.28 \times 10^{-7}$ [m^2·s^{-1}], $D = 0.256 \times 10^{-4}$ [m^2·s^{-1}], Le = 0.005, T_{oa} = 90^{o}C (363.15 K), T_{os} = 25^{o}C (298.15 K), h_{fg} = 2,442,300 [W·m^{-2}·^{o}C^{-1}], and ρ_a = 1/0.87 [kg·m^{-3}]. The results are obtained for the first fifteen eigenvalues. Also the results are obtained for various sets of the values of e and δ.

Figures 2, 3, and 4 illustrate that the variations of the air temperature with η_2 as time is variable for various sets of the values of e and δ. As it can be seen, by increasing time, the air temperature converges into a final constant value. In addition, by increasing the size of the system, the time required to converge into the final constant temperature is increased. For instance, for the case of e = 0.03 and δ = 0.09, the air temperature reaches its final constant value in approximately 20 min while for the case of e = 0.05 and δ = 0.15, it takes almost 4000 min to reach its final constant temperature.

Because the air temperature is larger than the solid temperature, the direction of heat transfer is from the air to the solid. So the air temperature is decreased as time increases. The slope of this decline is high for small values of η_2. The line of η_2 = 1 represents the temperature of the interface. By increasing time, due to the heat is exerted by the air, the temperature of the interface is slightly increased.

Figures 5, 6, and 7 show the variations of the solid temperature as a function of time for six different values of η_1 and for various sets of the values of e and δ. As

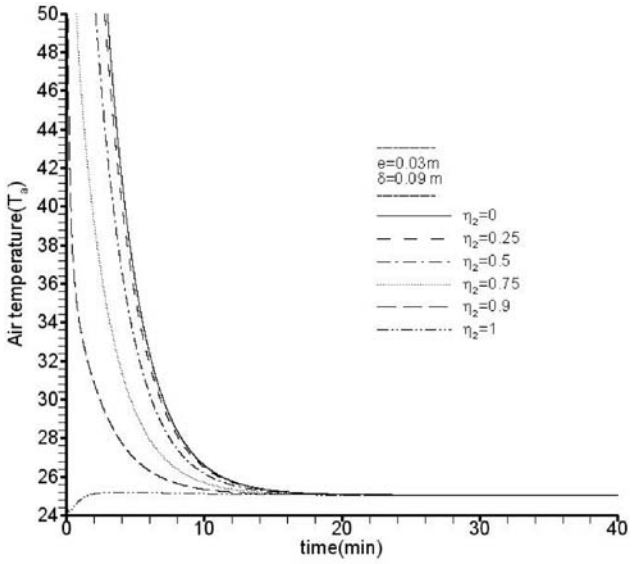

Fig. 2. Variation of air temperature with time at various η_2 at e = 0.03 and δ = 0.09.

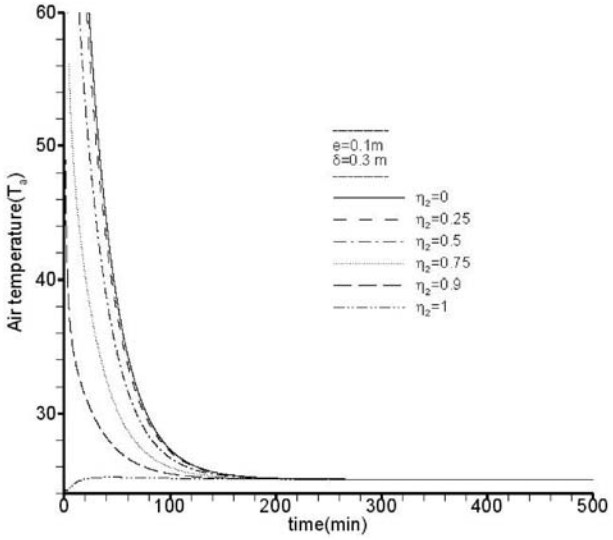

Fig. 3. Variation of air temperature with time at various η_2 at e = 0.1 and δ = 0.3.

shown in these figures, the solid temperatures at different values of η_1 become closer and closer to each other and approach toward a final common value. In addition, by increasing the size of the system, the time needed to approach toward the final common temperature is intensely increased. For example, in the case of e = 0.03 and δ = 0.09, the solid temperature reaches its final constant value in approximately 50 min while for the case of e = 0.05 and δ = 0.15, it takes almost 16,000 min to reach its final constant temperature.

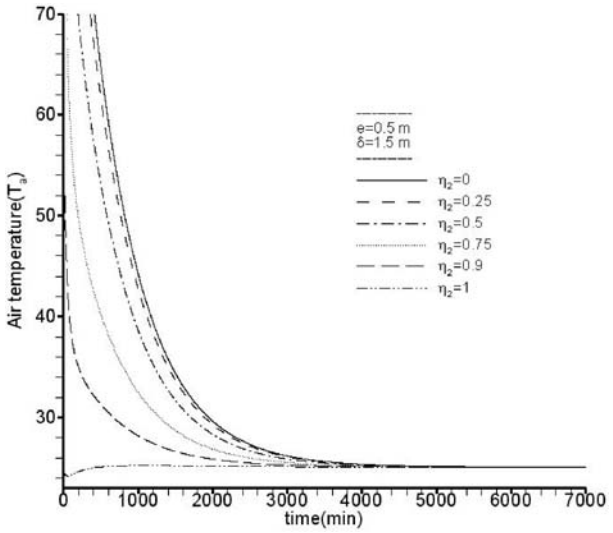

Fig. 4. Variation of air temperature with time at various η_2 at e = 0.5 and δ = 1.5.

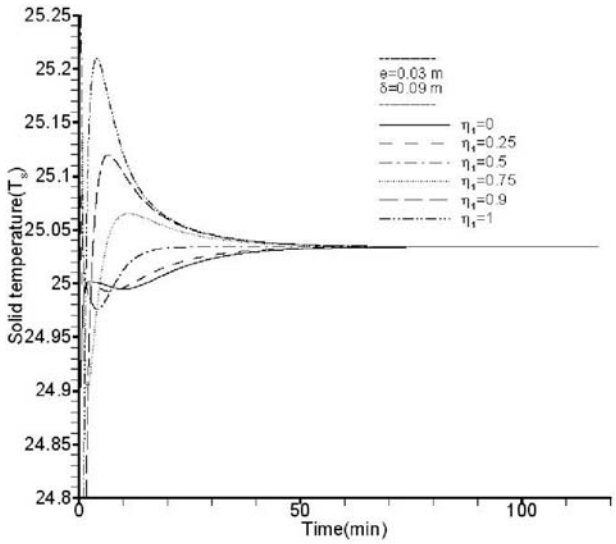

Fig. 5. Variation of the solid temperature with time at various η_1 at e = 0.03 and δ = 0.09.

At the top of the solid and near the interface (i.e., η_1 = 1, 0.9, and 0.75), for small values of time, the solid temperature is increased due to a high heat transfer rate from the air at small values of time. The line of η_1 = 1 represents the interface temperature similar to the line of η_2 = 1 in Figs. 2, 3, and 4. After that, the solid temperature is slightly decreased to approach toward a final common temperature. At the bottom of the solid (i.e., η_1 = 0, 0.25, and 0.5), the solid temperature is slightly increased toward the final common temperature.

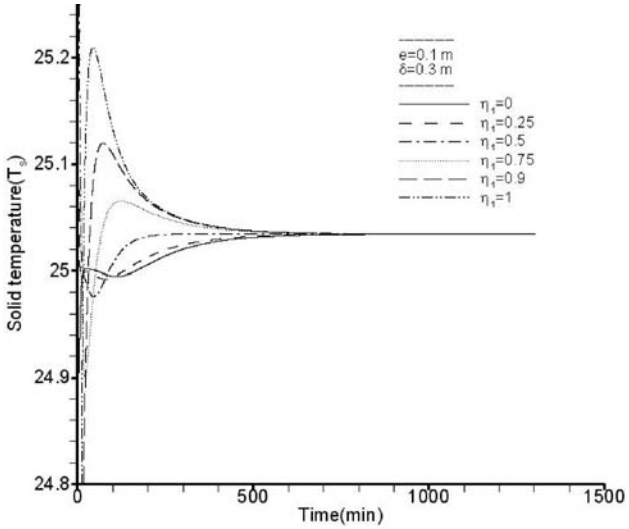

Fig. 6. Variation of the solid temperature with time at various η_1 at e = 0.1 and δ = 0.3.

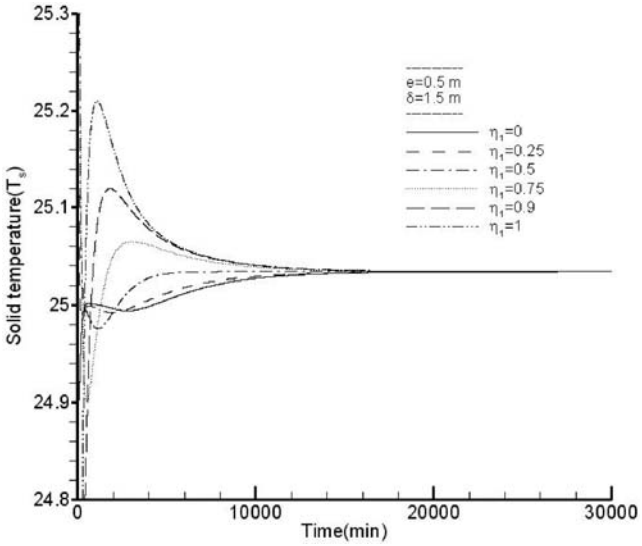

Fig. 7. Variation of the solid temperature with time at various η_1 at e = 0.5 and δ = 1.5.

Figures 8, 9, and 10 present the variations of the solid humidity as a function of time for six different values of η_1 and for various sets of values of e and δ. As it can be seen, in each figure, the solid humidity at each level converges into a final constant humidity. The time required to reach this final constant humidity increases by increasing the size of the system. For example, for the case of e = 0.03 and δ = 0.09, the solid is dried in approximately 25 min while for the case of e = 0.5 and δ = 1.5, the required time for drying is almost 600 min.

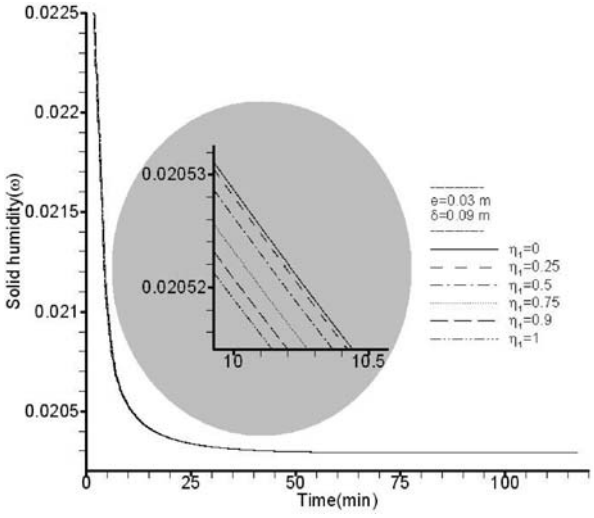

Fig. 8. Variation of the solid humidity with time at various η_1 at e = 0.03 and δ = 0.09.

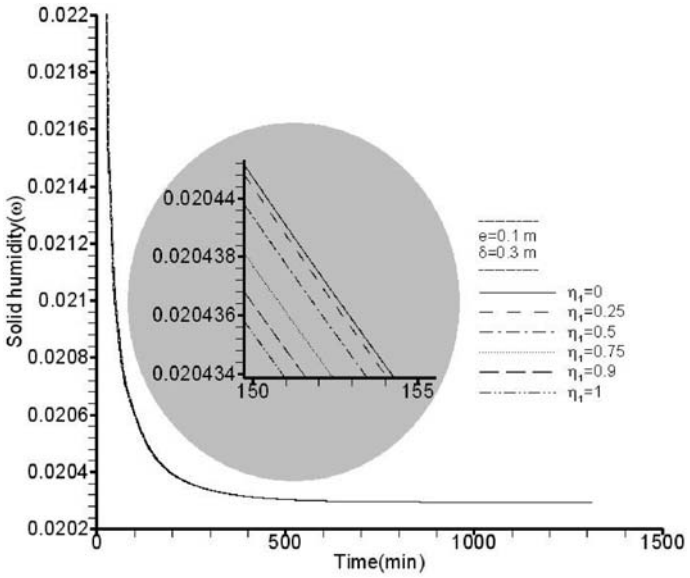

Fig. 9. Variation of the solid humidity with time at various η_1 at e = 0.1 and δ = 0.3.

In addition, due to heat transfer from the air to the solid, the solid humidity decreases by increasing time. Also, at each time, the solid humidity decreases by increasing η_1. So the minimum solid humidity is at the interface.

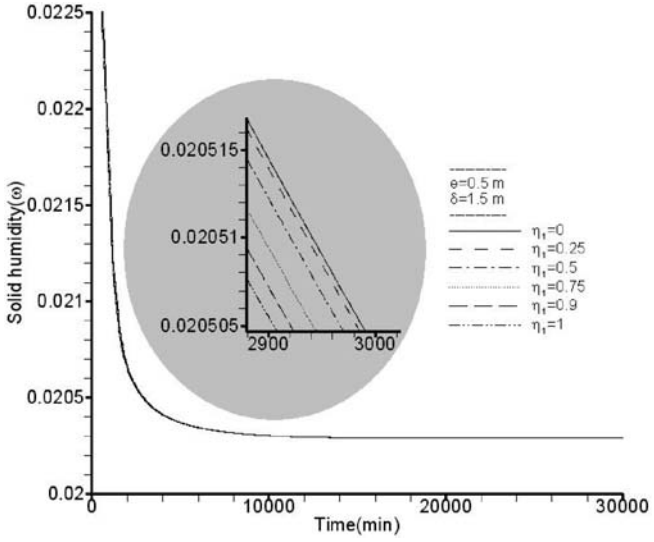

Fig. 10. Variation of the solid humidity with time at various η_1 at e = 0.5 and δ = 1.5.

6. CONCLUSIONS

Combined heat and mass transfer in industrial dryers is investigated analytically. At the solid and fluid interface, due to temperature and concentration gradients in the fluid and in the solid, heat and mass transfer exist between the solid and fluid phases. Because of these interfacial gradients, the governing equations are coupled at the interface. The unsteady heat and mass transfer equations are solved to obtain the distributions of the fluid and solid temperatures and the solid humidity. The results are obtained for various sets of values of e and δ.

The main results obtained can be summarized as follows:

1. By increasing time, the air and solid temperatures and the solid humidity converge into a final constant value. Each profile has a specific final constant value.
2. By increasing the size of a system, the time needed to converge into the final constant value increases. For instance, for the case of $e = 0.03$ and $\delta = 0.09$, the air temperature reaches its final constant value in approximately 20 min while for the case of $e = 0.05$ and $\delta = 0.15$, it takes almost 4000 min to reach its final constant temperature.
3. Since the air temperature is larger than the solid temperature, the direction of heat transfer is from the air to the solid and the air temperature decreases as time increases. The slope of this decrease is high for small values of η_2. During this process, the solid humidity and the fluid temperature decrease.
4. The line of $\eta_2 = 1$ in Figs. 2, 3, and 4 represents the interfacial temperature similar to the line of $\eta_1 = 1$ in Figs. 5, 6, and 7. By increasing time, due to the heat exerted by the air, the interfacial temperature increases slightly.

NOMENCLATURE

A_n, B_n, C_n	coefficients in Eqs. (24), (25) and (26)
D	effective diffusivity, m^2/s
E	thickness of solid space, m
F_n, G_n, H_n	eigenfunctions in Eqs. (35), (36), and (37)
h_{fg}	latent heat of vaporization, J/kg
K	thermal conductivity of air, W/(m·K)
Le	Lewis number, $= \alpha_s/D$
P	pressure, Pa
T	temperature, K or ^oC
t	time, s
x, y_1, y_2	coordinate directions, m

Greek symbols

α	thermal diffusivity, m^2/s
α_n, β_n, γ_n	eigenvalues in Eqs. (24), (25) and (26)
ρ	density, kg dry air/m^3

δ	thickness of fluid space, m
τ	normalized time
η	normalized coordinate
θ	normalized temperature
ω	humidity of solid, kg/kg dry air
ϖ	normalized humidity
$\lambda_1, \lambda_2, \lambda_3, \lambda_4$	constant parameters

Subscripts

a	air (fluid)
s	solid
e	equilibrium condition
oa	initial condition of fluid
os	initial condition of solid
sat	saturated condition
int	interface condition.

REFERENCES

Arnaud, G. and Fohr, J. P., Slow drying simulation in thick layers of granular products, *Int. J. Heat Mass Transfer*, vol. 31, pp. 2517–2526, 1988.

Ashworth, J. C., The mathematical simulation of batch-drying of softwood timber, Ph.D. thesis, University of Canterbury, New Zealand, 1977.

Bruhat, G., *Thermodynamique*, 6th Ed., Paris: Masson, 1968.

Grossman, G., Simultaneous heat and mass transfer in falling film absorption under laminar flow, *Int. J. Heat Mass Transfer*, vol. 26, pp. 357–371, 1983.

Ibrahim, G. A. and Vinnicombe, G. A., A hybrid method to analyze the performance of falling film absorbers, *Int. J. Heat Mass Transfer*, vol. 36, pp. 1383–1390, 1993.

Iskra, C. R. and Simonson, C. J., Convective mass transfer coefficient for a hydrodynamically developed airflow in a short rectangular duct, *Int. J. Heat Mass Transfer*, vol. 50, pp. 2376–2393, 2007.

Johansson, A., Fyhr, C., and Rasmuson, A., High temperature convective drying of wood chips with air and superheated steam, *Int. J. Heat Mass Transfer*, vol. 40, pp. 2843–2858, 1997.

Killion, J. D. and Garimella, S., A critical review of models of coupled heat and mass transfer in falling-film absorption, *Int. J. Refrig*., vol. 24, pp. 755–797, 2001.

Kulasiri, D. and Woodhead, I., On modeling the drying of porous materials: analytical solutions to coupled partial differential equations governing heat and moisture transfer, *Math. Probl. Eng*., vol. 3, pp. 275–291, 2005.

Le Palec, G., Numerical study of heat and mass transfer from an inclined flat plate with wet and dry zones, *Int. J. Heat Mass Transfer*, vol. 35, pp. 2277–2287, 1992.

Li, Y., Klausner, J. F., Mei, R. and Knight, J., Direct contact condensation in packed beds, *Int. J. Heat Mass Transfer*, vol. 49, pp. 4751–4761, 2006.

Luikov, A. V., *Heat and Mass Transfer in Capillary-Porous Bodies*, Pergamon Press, 1966.

Mujumdar, Arun S., *Handbook of Industrial Drying*, Dekker, 1995.

Olbrich, W. E. and Wild, J. D., Diffusion from the free surface into a liquid film in laminar flow over defined shapes, *Chem. Eng. Sci*., vol. 24, pp. 25–32, 1969.

Olutimayin, S. O. and Simonson, C. J., Measuring and modeling vapor boundary layer growth during transient diffusion heat and moisture transfer in cellulose insulation, *Int. J. Heat Mass Transfer*, vol. 48, pp. 3319–3330, 2005.

Papia, S., Wijeysundera, N. E., Ho, J. C., and Yap, C., Modeling of horizontal tube-bundle absorbers of absorption cooling systems, *Int. J. Refrig*., vol. 30, pp. 709–723, 2007.

Raisul Islam, Md., Wijeysundera, N. E. and Ho, J. C., Heat and mass transfer effectiveness and correlations for counter-flow absorbers, *Int. J. Heat Mass Transfer*, vol. 49, pp. 4171–4182, 2006.

Talukdar, P., Iskra, C. R., and Simonson, C. J., Combined heat and mass transfer for laminar flow of moist air in a 3D rectangular duct: CFD simulation and validation with experimental data, *Int. J. Heat Mass Transfer*, vol. 51, pp. 3091–3102, 2008.

Thomas, H. R., Morgan, K., and Lewis, R. W., A fully nonlinear analysis of heat and mass transfer problems in porous bodies, *Int. J. Numer. Meth. Eng*., vol. 15, no. 9, pp. 1381–1393, 1980.

van Arsdel, W. B., Copley, M. J., and Morgan, A. I., *Food Dehydration*, Vol. 1, Westport, CT, USA: AVI Publ. Co., Inc., 1973.

Williams-Gardner, A., *Industrial Drying*, London: Leonard Hill, 1971.

□◆◆◆□